ORIGINAL ARTICLE

Cellular, biochemical and molecular changes in muscles from patients with X-linked myotubular myopathy due to *MTM1* mutations

Christoph Bachmann[1], Heinz Jungbluth[2,3,4], Francesco Muntoni[5], Adnan Y. Manzur[5], Francesco Zorzato[1,6] and Susan Treves[1,6,*]

[1]Departments of Biomedicine and Anesthesia, Basel University Hospital, Basel University, Basel, Switzerland, [2]Department of Paediatric Neurology, Neuromuscular Service, Evelina Children's Hospital, St Thomas' Hospital, London, UK, [3]Department of Basic and Clinical Neuroscience, Institute of Psychiatry, Psychology and Neuroscience (IoPPN), King's College London, London, UK, [4]Randall Division of Cell and Molecular Biophysics, Muscle Signalling Section, King's College, London, UK, [5]Dubowitz Neuromuscular Centre and MRC Centre for Neuromuscular Diseases, Institute of Child Health, London, UK and [6]Department of Life Sciences, General Pathology section, University of Ferrara, Ferrara, Italy

*To whom correspondence should be addressed at: Susan Treves, lab 408 Department of Anesthesia and Biomedicine, Hebelstrasse 20, 4031 Basel, Switzerland. Tel: +41612652373; Fax: +41612653702; Email: susan.treves@unibas.ch

Abstract

Centronuclear myopathies are early-onset muscle diseases caused by mutations in several genes including *MTM1*, *DNM2*, *BIN1*, *RYR1* and *TTN*. The most severe and often fatal X-linked form of myotubular myopathy (XLMTM) is caused by mutations in the gene encoding the ubiquitous lipid phosphatase myotubularin, an enzyme specifically dephosphorylating phosphatidylinositol-3-phosphate and phosphatidylinositol-3,5-bisphosphate. Because XLMTM patients have a predominantly muscle-specific phenotype a number of pathogenic mechanisms have been proposed, including a direct effect of the accumulated lipid on the skeletal muscle calcium channel ryanodine receptor 1, a negative effect on the structure of intracellular organelles and defective autophagy. Animal models knocked out for *MTM1* show severe reduction of ryanodine receptor 1 mediated calcium release but, since knocking out genes in animal models does not necessarily replicate the human phenotype, we considered it important to study directly the effect of *MTM1* mutations on patient muscle cells. The results of the present study show that at the level of myotubes *MTM1* mutations do not dramatically affect calcium homeostasis and calcium release mediated through the ryanodine receptor 1, though they do affect myotube size and nuclear content. On the other hand, mature muscles such as those obtained from patient muscle biopsies exhibit a significant decrease in expression of the ryanodine receptor 1, a decrease in muscle-specific microRNAs and a considerable up-regulation of histone deacetylase-4. We hypothesize that the latter events consequent to the primary genetic mutation, are the cause of the severe decrease in muscle strength that characterizes these patients.

Introduction

Centronuclear myopathies are rare muscle disorders caused by mutations in several genes including *MTM1*, *DNM2*, *BIN1*, *RYR1* and *TTN* (1–7) and are associated with autosomal dominant, autosomal recessive and X-linked modes of inheritance. The X-linked form (XLMTM, MIM #310400) is the most severe and is characterized by profound muscle weakness, severe bulbar and respiratory involvement. Symptoms are typically present at birth and without ventilator support most affected males die within the first year of life, though some infants have a milder presentation with less severe onset and survive into early childhood or adolescence (1,2,8,9). Muscle biopsies typically show the presence of numerous centralized nuclei, the predominance of often atrophic type I fibres, disorganization of the myofibrillar network and, particularly in more mildly affected males and manifesting females, 'necklace fibres' (10–12). *MTM1* encodes for myotubularin, a lipid phosphatase that specifically dephosphorylates phosphatidylinositol-3-phosphate (PI(3)P) and phosphatidylinositol-3,5-bisphosphate (PI(3,5)P$_2$) to produce PI and PI(5)P, respectively (for review see 3). Though myotubularin is ubiquitously expressed, mutations in the *MTM1* gene result in a selective skeletal muscle phenotype. One reason for this may be the lack of expression of potentially compensatory myotubularin related proteins in skeletal muscle in contrast to their expression in other tissues (13); however, skeletal muscles expresses MIP/MTMR14 a phosphatidylinositol phosphate phosphatase of apparent similar function as myotubularin and mice knocked out for MIP/MTMR14 also exhibit a severe muscle phenotype (14), raising the possibility that altered phosphatidylinositol lipid metabolism specifically interferes with physiological skeletal muscle function(s) and/or development (15). To date more than 200 different *MTM1* mutations (including missense, frameshift and small deletions) have been identified in XLMTM patients with most mutations predicted to affect enzymatic activity (9,10,16–19).

In humans, 15 genes encode for different myotubularins with most members of this family playing important roles in membrane trafficking, movement of intracellular vesicles, autophagy and phagocytosis (3,20–22). In addition to their role as phosphatases, myotubularins also contain functional domains promoting protein-protein or lipid-protein interactions suggesting that the lack of the myotubularin complex may additionally be involved in disease pathogenicity (18,19). Muscles from 5 week old *Mtm1*-null mice are 50% lighter compared to controls, show disorganization of triadic architecture, longitudinally oriented tubules and a significant decrease in RyR1 and Ca$_v$1.1 protein content (23). Furthermore, *Mtm1*-null mice and zebrafish exhibit abnormal Ca^{2+} homeostasis and impaired excitation-contraction coupling (ECC) (13,23). ECC is the process occurring in striated muscles whereby an electrical signal, the depolarization of the plasma membrane, is converted into a chemical signal, that is an increase in the myoplasmic calcium concentration, leading to muscle contraction (24,25). The two key players of skeletal muscle ECC are the dihydropyridine receptor (DHPR), a multi-protein complex made up of 5 subunits (Ca$_v$1.1, ß1, γ, α1, α2, and ∂) (26) which is localized on the transverse tubules where it acts as a voltage sensor and the ryanodine receptor (RyR1), a macromolecular complex of > 2.5 MDa made up of 4 homotetramers, that constitute the Ca^{2+} release channel of the sarcoplasmic reticulum (SR) (24,27). Activation of the DHPR induces conformational changes that promote its interaction with the RyR1; this leads to the opening of the RyR1 and to the release of Ca^{2+} from the SR stores. In order to occur

rapidly (few milliseconds) and efficiently, ECC relies on a highly sophisticated and well-defined subcellular architecture with each DHPR facing a RyR1 in a highly organized conformation (24,27) thus a reduction of the RyR1 protein content or disorganization of triadic architecture should negatively affect ECC. Indeed, patients with recessive *RYR1* mutations exhibiting a severe reduction in RyR1 protein content are affected by congenital muscle disorders (28–30), and animal models knocked out for structural SR proteins show reduced muscle strength (31–33). In a recent study, we investigated the mechanism leading to reduced RyR1 expression in patients with recessive *RYR1*-related congenital myopathies and found that a pathological epigenetic loop involving changes in the expression of microRNAs and class II histone deacetylases (HDACs) is activated (34). Since muscles from *Mtm1*-null mice show reduced RyR1 expression, we hypothesize that similar epigenetic changes might occur in the muscles of patients with XLMTM.

In the present study, we investigated the physiological, biochemical and epigenetic characteristics of skeletal muscles from patients with *MTM1* mutations. Surprisingly ECC in myotubes from *MTM1*-mutated patients was unaffected while there were important biochemical and epigenetic modifications occurring in mature muscle fibres. The findings of this and of our recent study (34) indicate that common epigenetic changes consequent to the primary genetic defect are activated in different congenital myopathies. Targeting such secondary modifications could potentially improve the muscle function in patients affected by congenital myopathies with the common feature of the reduced RyR1 protein content.

Results

Patient description

The genotypic and phenotypic characteristics of the patients enrolled in the present study are shown in Table 1. Five of six patients either had frameshift mutations, deletions or premature stop codons and only one patient (NH14-1816) carried a missense mutation. The recurrent p.Arg241Cys mutation shows phenotypic variation and has previously been identified in severely, moderately and mildly affected patients (16–19). The patient carrying the p.Arg241Cys mutation investigated in this study was severely affected, requiring ventilation and a tracheostomy. Surprisingly, patient N° 6499 who carried a 2 nucleotide deletion in exon 14 which encodes part of the SID (SET interaction domain) was only moderately affected; he was nasogastric tube/gastrostomy fed, did not require ventilator support, achieved the ability to sit unsupported, but had swallowing difficulty with oral secretions and suffered a respiratory arrest at age three. Three patients died at 4, 6 months and 3 years. Three patients are >1 year old but are severely affected and require mechanical ventilation. These results are in line with previous reports suggesting that in general, truncating mutations are associated with a severe phenotype. In order to verify whether potential genotype-phenotype correlations could be identified at the molecular level, we investigated physiological, cellular and biochemical changes occurring in the muscle cells of the affected patients.

Immunohistochemistry and functional studies on primary muscle cells

PI phospholipids are present in specific subcellular membrane compartments and organelles and alterations in their

Table 1. Genotype and phenotype of the patients investigated in the present study

| Sample ID	Disease severity	Phenotype	Exon	MTM1 mutation	Amino acid substitution
NH15-0805	Severe	Ventilator dependent aged 18 months.	11	c.1084_1087delGACA	p.Asp362fs
6212	Severe	Died aged 4 months	11	c.1171T>G	p.Tyr397X
NH13-0078	Severe	Died age of 6 months, Bipap ventilated.	8	c.594C>G	p.Tyr198X
6499	Moderate	Neonatal nasogastric tube requirement and gastrostomy and one year. Ventilation not required, but marked orobulbar secretions difficulties. Died at 3 years 10 months age.	14	c.1508_1509delAC	
7457	Moderate/Severe	Non-invasive mask ventilation at 3 months, tracheostomy by 1 year. 24 h tracheostomy ventilation dependent at age 12 years.	1	deletion exon1 and 5' part of gene	
NH14-1816	Severe	Ventilator dependent via tracheostomy aged 2 years. No head control or sitting ability.	9	c.721C>T	p.Arg241Cys

distribution and content may affect cell size, growth and appearance. We first examined the gross morphology of differentiated myotubes form healthy controls and patients harbouring *MTM1* mutations. Muscle cells were only available from patients having either a frameshift mutation, deletion of the 5'end of the gene, or a premature stop codon (Supplementary Material, Table S1) all of which are expected to result in lack of myotubularin protein expression. Figure 1A shows a brightfield image of the cells from a healthy control (top panel) and a patient (bottom panel), and panels B-D show the average area, number of nuclei and nuclei/area, respectively. As shown myotubes from the XLMTM patients were significantly smaller and had fewer nuclei than myotubes from healthy controls, though the number of nuclei/cell area remained unchanged. These results suggest that the lack of myotubularin negatively affects cell growth.

Since there are no commercial antibodies recognizing PI(3,5)P_2, one of the substrates of myotubularin, we performed immunofluorescence analysis on myotubes to check for alterations in the subcellular distribution and content of PI3P as well as PI(3,4)P_2, a PI that can either be phosphorylated to yield PI(3,4,5)P_3 or dephosphorylated to yield PI4P and then potentially re-converted to PI3P (35). Figure 2 shows the localization of the two phospholipids in myotubes from a healthy control (Fig. 2A panels a and e) and a patient with XLMTM (Fig. 2A panels c and g). Panels b, d, f and h of Fig. 2 show the cellular distribution of actin (phalloidin, green), the PI phospholipid (red) and nuclei (DAPI, blue). The commercial antibodies against the two phospholipids show background staining on areas of the coverslips devoid of any cells; these may be either lipid aggregates or fragments of the membranes of cells that have detached. Nevertheless there is a punctuated staining in correspondence of the myotubes and as far as the gross appearance and distribution of the phospholipids is concerned, these were similar in control and patient myotubes, with PI3P having a punctuated, uniformly distributed fluorescence within a membrane compartment, and PI(3,4)P_2 having a more patchy appearance, concentrated within particular membrane domains. More detailed examination revealed quantitative differences in the amount of PI3P present as determined by fluorescence intensity; in particular there was ∼ a 2 fold increase in the mean fluorescence intensity (measured as arbitrary units) associated with PI3P but

no significant change in the level of PI(3,4)P_2 in myotubes from patients versus controls (Fig. 2B).

In muscle fibres from *Mtm1*-null zebrafish and 5 weeks old *Mtm1*-null mice profound changes in the distribution of RyR1 and $Ca_v1.1$ have been described, with the absence of immunolabelling in some regions and disruption of the triad architecture (13,23). We therefore examined the distribution of RyR1 and $Ca_v1.1$ in patient myotubes; even though the latter cells do not achieve the degree of differentiation typical of mature fibres (36), a drastic decrease or mis-localization of these proteins would be observable by confocal microscopy. However, no substantial changes in the subcellular distribution of RyR1 (Fig. 3A, panels a and d) and $Ca_v1.1$ (Fig. 3A panels b and e) were observed. More importantly, quantification of RyR1 and $Ca_v1.1$ protein by Western blot revealed that if anything, the content of these two proteins was increased in myotubes from patients compared to controls (Fig. 3B and C). Figure 3B and C also show that the protein content of HDAC-4 is similar in myotubes from controls and patients while the protein myotubularin is present in myotubes from healthy controls but is absent from myotubes from XLMTM patients (Fig. 3B and C).

In previous reports it was shown that muscle fibres from the *Mtm1*-null mice show impaired ECC (23). In order to verify if this was also the case in cells from human *MTM1*-mutant patients we investigated the calcium homeostasis and ECC characteristics of myotubes from 3 patients (2 carrying frameshift mutations and 1 carrying a premature stop codon) and compared them to those of myotubes from healthy controls (pooled results from 3 different individuals). There was a small but significant decrease in the resting $[Ca^{2+}]_i$ in myotubes from patients harbouring *MTM1* mutations (Fig. 4A), whereas the total amount of rapidly releasable Ca^{2+} within intracellular stores calculated as area under the curve (AUC) after addition of 1 μM thapsigargin and 1 μM ionomycin in Krebs Ringer containing 100 μM La^{3+} and 0.5 mM EGTA (34,36), was similar in control and patient myotubes (Fig. 4B). Figure 4C shows a representative trace of changes in the $[Ca^{2+}]_i$ in response to 60 mM KCl in Krebs Ringer containing 100 μM La^{3+}. The peak Ca^{2+} elicited by 600 μM 4-cmc and 60 mM KCl (Fig. 4D and E, respectively) were similar in myotubes from controls and patients. There were no significant differences in the dose response curves to 4-cmc and KCl (see also Supplementary Material, Fig. 1), the EC$_{50}$ being 351.4 ± 65.6 and
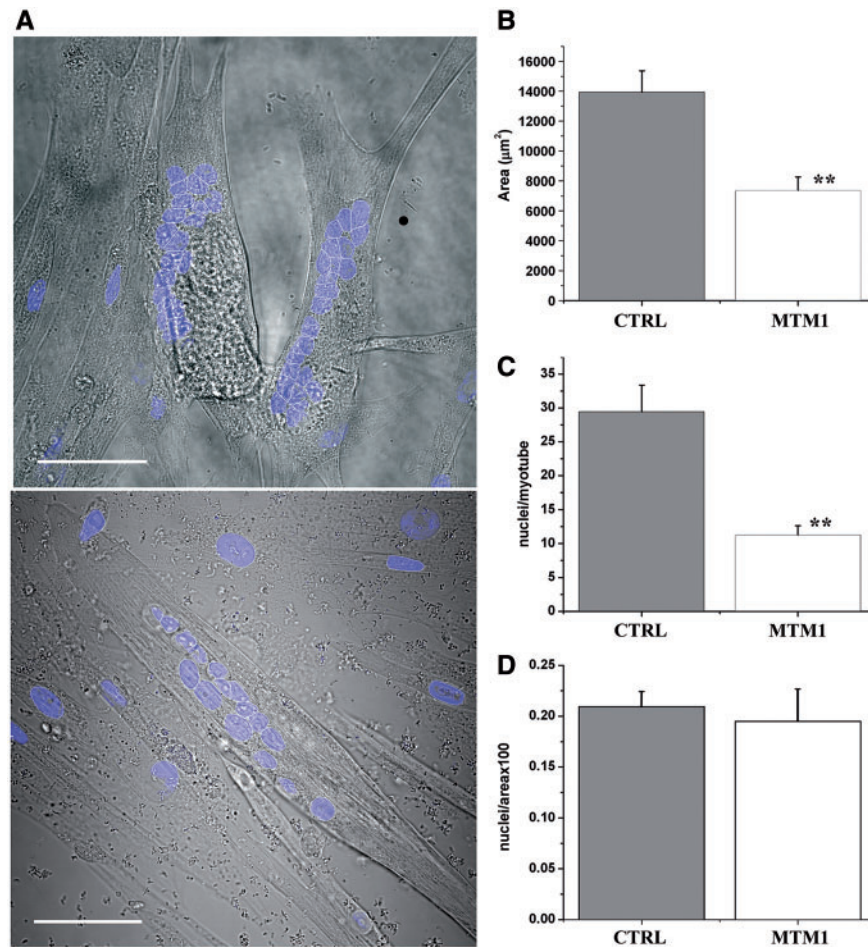
Figure 1. Myotubes from XLMTM patients are smaller and have fewer nuclei than myotubes from healthy **controls**. (**A**) Brightfield image overlaid with DAPI staining to visualize nuclei. Top panel shows myotubes from a healthy control, bottom panel, from a patient with XLMTM; bar indicates 50 μm. (**B**) Mean (±SEM) myotube area and (**C**) mean (±SEM) number of nuclei/myotube was significantly higher in cells from controls (total number of cells measured = 41) compared to cells from XLMTM patients (total number of cells measured = 16). (**D**) The calculated ratio of number of nuclei/cell area was not different. Cells were prepared as described in the Materials and Methods section, fixed with paraformaldehyde and stained with DAPI to visualize nuclei with a Plan Fluor 20x air objective (NA 0.75). **P < 0.01 Student's *t* test.

387.4 ± 33.7 μM for 4-cmc and 16.1 ± 4.2 and 12.0 ± 3.8 mM for KCl in control and patient myotubes, respectively. In conclusion, these results indicate that at the level of myotubes, mutations in *MTM1* cause a 2 fold increase in PI3P, a decrease in myotube size and nuclear content but no major alterations in the distribution of PI3P/PI(3,4)P$_2$, nor in the proteins involved in ECC. In the next series of experiments, we investigated if biochemical changes were occurring in mature patient muscle fibres.

Biochemical analysis and epigenetic modifications in muscles from patients with XLMTM

The content of RyR1, Ca$_v$1.1 and class II histone deacetylases (HDAC-4 and HDAC-5) was investigated by immunoblotting on total muscle homogenates from patients and healthy controls. We assessed class II HDACs since a decrease in the RyR1 protein level was observed in the muscle of patients with CNM due to recessive *RYR1* mutations and this is accompanied by a significant increase in HDAC-4 and HDAC-5 protein content (34). Figure 5A and C shows representative Western blots and Fig. 5B and D shows the relative protein content of RyR1 and Ca$_v$1.1

normalized to MyHC content. The anti-MyHC antibody that was used recognizes all isoforms, so that the results are not affected by the potential expression of different MyHC isoforms. Protein quantification could not be performed on biopsies from all patients due to the lack of sufficient biological material. Nevertheless, qPCR analysis was performed on muscle samples from all patients (see next paragraph). The results depicted in Fig. 5A–D confirm that both RyR1 and Ca$_v$1.1 protein content was significantly reduced in most mature human *MTM1*-mutated muscle fibres whereas the levels of HDAC-4 were significantly increased, while those of HDAC-5 were not as elevated. Of interest, patient NH13-0078 carrying the p.Tyr198X mutation had RyR1 and HDAC-4 protein levels that were similar to those of controls, whereas the moderately affected patient carrying the c.1508_1509 deletion (N° 6499) had HDAC-4 protein levels that were >200 times higher than in controls. Protein and transcript levels were not always concordant (see next paragraphs).

In patients with recessive *RYR1* mutations increased class II HDAC content was paralleled by an increase in the transcripts encoding DNA methyltransferase 1 (*DNMT1*), and DNA methyltransferases 2 (now called tRNA aspartic acid methyltransferase 1, or *TRDMT1*) (34). We therefore also investigated whether similar changes occur in the muscles of patients with *MTM1*
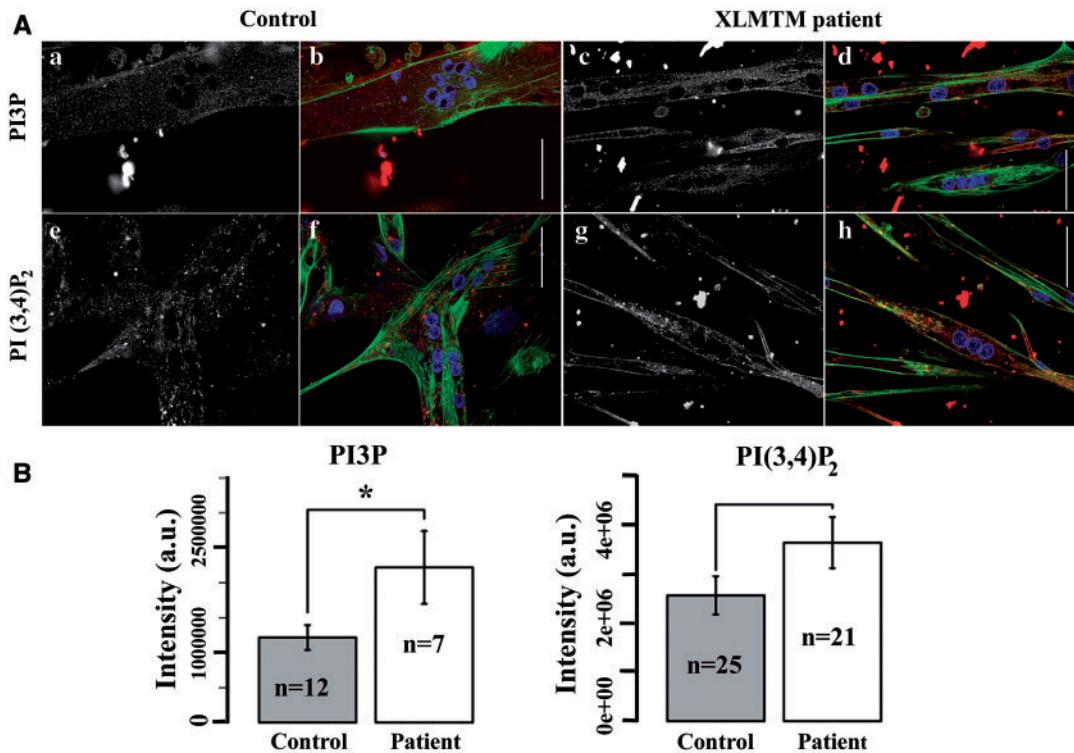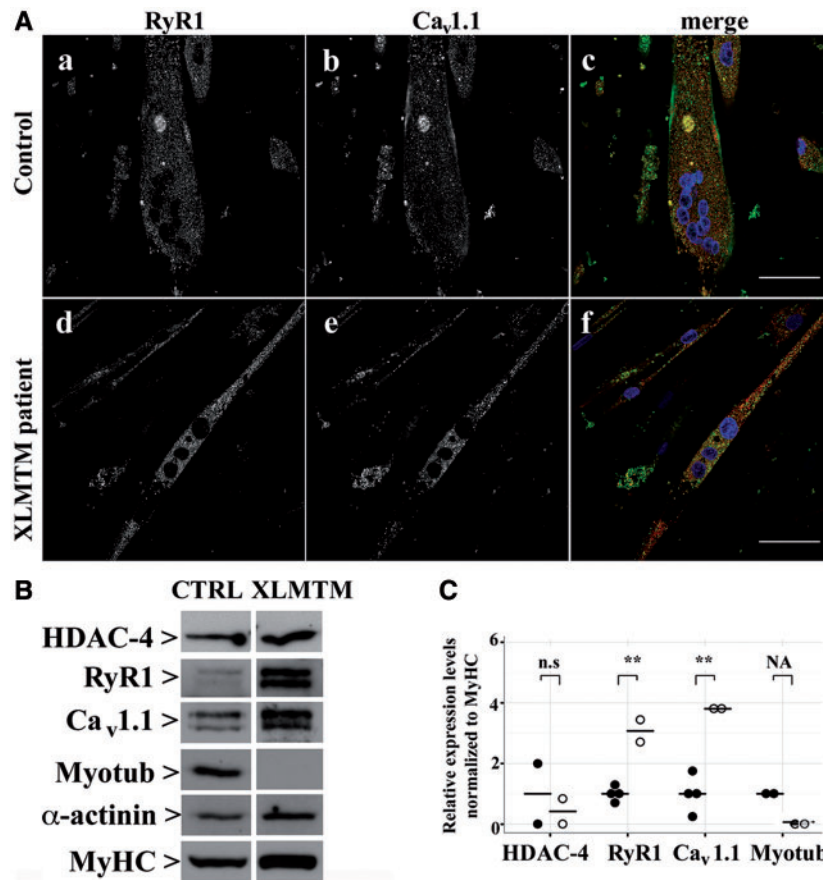
Figure 2. The subcellular distribution of PI3P and PI(3,4)P_2 in myotubes is similar in cells from XLMTM patients and healthy controls. Human skeletal muscle myotubes were stained as described in the Material and Methods section and analysed using a Nikon A1 plus confocal microscope equipped with a Nikon Plan Apo TIRF 60x oil objective (NA 1.49). (**A**) Subcellular distribution of PI3P in myotubes from a healthy control (**a**) and an XLMTM patient (**c**). Subcellular distribution of PI(3,4)P_2 in myotubes from a healthy control (**e**) and an XLMTM patient (**g**). Composite images showing the distribution of PI3P (red), actin (green) and nuclei (blue) in myotubes from a healthy control (**b**) and an XLMTM patient (**d**). Composite images showing the distribution of PI(3,4)P_2 (red), actin (green) and nuclei (blue) in a myotube from a healthy control (**f**) and an XLMTM patient (**h**). The background staining on areas of the coverslip devoid of cells may be caused either by lipid aggregates or by fragments of membranes of cells that have detached. Also note that the subcellular distribution of the two phospholipids is different: PI3P has a punctuate uniform intracellular membrane distribution whereas PI(3,4)P_2 appears to be more clustered within intracellular membranes. Bar indicates 50 μm. (**B**) Bar chart showing the mean (±S.E.M.) fluorescence intensity (arbitrary units, a.u.) associated with PI3P and PI(3,4)P_2 in myotubes from a control and XLMTM patient. *$P < 0.05$ Student's *t* test.

mutations. Figure 5E shows that a significant increase (approximately 10 fold) in both in *DNMT1* and *TRDMT1* transcripts occurs in the muscles of the XLMTM patients. Note that in Fig. 5E the values for patients 0805 and 7457 have not been plotted since they were >1000 fold higher than in control muscles; however, all expression values are presented in panel F of Fig. 5 where the expression levels of the transcripts encoding *HDAC4, RYR1, MTM1, DNMT1* and *TRDMT1* of each patient compared to levels observed in biopsies from control individuals are shown. The latter values were used as a reference and set to 1 (Fig. 5F). A decrease in the transcript is indicated in red and an increase in green and the colour-code scale is shown in the right hand column. *RYR1* transcripts were significantly reduced by more than 50% in muscle biopsies from all patients examined and *HDAC4* transcripts were significantly elevated in all patients. The increase in *HDAC4* was paralleled by increased expression of the DNA methylating enzyme transcripts *DNMT1* and *TRDMT1*. Of note, patients 0805 and 7457 were particularly striking since they exhibited >40 fold increased levels of *MTM1*, the highest levels of *HDAC4* transcripts and >700 fold levels of *DNMT1* and *TRDMT1*. Curiously, at the myotube level HDAC-4 was expressed to similar levels in myotubes from healthy controls and XLMTM patients (see Fig. 3 panels B and C) indicating that these epigenetic modifications only occur in the mature muscle tissue.

As mentioned above, the relative expression of HDAC-4 protein and transcript level did not always correlate, particularly in the case of patient 6499 where HDAC-4 protein was elevated

approximately 200 fold but whose transcript was increased only 3 times. Similar discrepancies were found for *MTM1* transcript and protein levels: mRNA levels were decreased in 3 patients (N° 6212, 0078 and 6499) and increased in 3, (N° 1816, 0805 and 7457) whereas the myotubularin protein was absent in the muscles of patients N° 6212, 0805 and 0078 (Supplementary Material, Fig. 2A). Insufficient quantities of biological material precluded the assessment of myotubularin protein in the biopsies from the remaining patients. PI3P levels were significantly elevated in muscles of all XLMTM patients tested (patients N° 0078, 1816, 0805, 6212 and 6499. Supplementary Material, Fig. 2B) confirming the results obtained on myotubes (Fig. 2) as well as the previous observation that cells from patients or animal models knocked out or knocked in for human *MTM1* mutations have higher PI3P levels (13,23,37,38).

We focused the next series of experiments on determining the content of microRNAs (miRs). Because of the limited amount of biological material, we measured the expression levels of a selected group of muscle-specific miR transcripts, namely miR-1, miR-133, miR-206 and the muscle enriched miR-486 as well as miR-22, miR-124 which are predicted to bind to the 3'UTR of the *RYR1* gene and several miRs predicted to bind to the human *MTM1*. Figure 6 shows the mean expression levels and Supplementary Material, Table S2 shows miR levels in individual patients. As shown, most miRs were significantly down-regulated, except for miR-124, 128 and 206 that showed greater variability and were not always changed when compared to

Figure 3. Cellular distribution and quantification of RyR1 and $Ca_v1.1$ in differentiated myotubes from XLMTM patients and healthy controls. (**A**) Confocal analysis of subcellular distribution of RyR1 and $Ca_v1.1$ in myotubes. Human myotubes were visualized with a Nikon A1 plus confocal microscope equipped with a Plan Apo 60x oil objective (NA 1.49) and stained as described in the Materials and Methods section. Top panels show myotubes from a healthy control, bottom panels show myotubes from an XLMTM patient. Panels (**a**) and (**d**) anti-RyR1, panels (**b**) and (**e**) anti-$Ca_v1.1$. Panels (**c**) and (**f**) composite image of anti-RyR1 (red), anti-$Ca_v1.1$ (green) and DAPI (blue); orange pixels show area where RyR1 and $Ca_v1.1$ co-localize. Bar indicates 50 μm. (**B**) Representative immunoblots of myotubes from a control and XLMTM patient. Blots were probed with the indicated primary antibodies. (**C**) Relative content of the immunopositive band (normalized to MyHC) of HDAC-4, RyR1, $Ca_v1.1$ and myotubularin (MTM1) in myotubes from controls (full circles) and XLMTM patients (empty circles). **Student's t test $P < 0.01$; n.s. not significantly different. NA, not applicable.

levels in biopsies from healthy controls. Of interest patients N° 1816, 0805 and 7457 who were all severely affected showed down-regulation of all the miRs, down-regulation of *RYR1* transcript and up-regulation of *HDAC4* transcript.

Muscles from XLMTM patients are different from foetal muscles

Data from the literature suggest that muscles from XLMTM patients revert to a 'foetal' phenotype (15) a hypothesis that is compatible with the up-regulation of HDAC-4 and down-regulation of RyR1 and of muscle-specific miRs. Since we had available small amounts of muscle samples from non-affected 13.8–20.2 week old foetuses, we used these to assess the content of several proteins. Not unexpectedly the foetal samples contain very high levels of HDAC-4 protein (Supplementary Material, Fig. 3) and HDAC-5 but because of the large variability and small sample size this did not achieve statistical significance (Fig. 7A); on the other hand, the relative content of RyR1 was significantly reduced while that of $Ca_v1.1$ was either unchanged (1 sample) or reduced (1 sample) (Fig. 7B).

Since the MyHC isoform expressed by a muscle is a sensitive and accepted indicator of muscle fibre type we performed high-resolution gel electrophoresis on control, foetal and patient muscle extracts to verify their degree of development, using conditions that allow separation of the different MyHC isoforms (39,40). Figure 7C shows a representative gel stained with Coomassie Blue showing the separation of MyHC isoforms (I, IIa and IIx) in human muscle biopsies. As shown the muscle sample from a control shows the 3 bands corresponding to MyHC I, IIa and IIx, while in foetal muscle the MyHC I band corresponding to the slow isoform is clearly present, together with a band having an electrophoretic mobility similar to that of MyHC IIa. The MyHC isoform present in muscle biopsies from the 5 patients carrying *MTM1* mutations were not uniform, showing the presence of bands having different electrophoretic mobility, with the biopsy from patient MTM1 0805 being more similar to that of the control individual. The upper band present in foetal muscle (and in the muscles from the XLMTM patients) having an electrophoretic mobility similar to MyHC IIa, may correspond to the embryonic/foetal isoform. We therefore also performed a Western blot using an antibody specific for MyHC3 (embryonic/ foetal isoform). Figure 7D shows that MyHC3 is virtually absent from control muscles, whereas a strong immunoreactive band
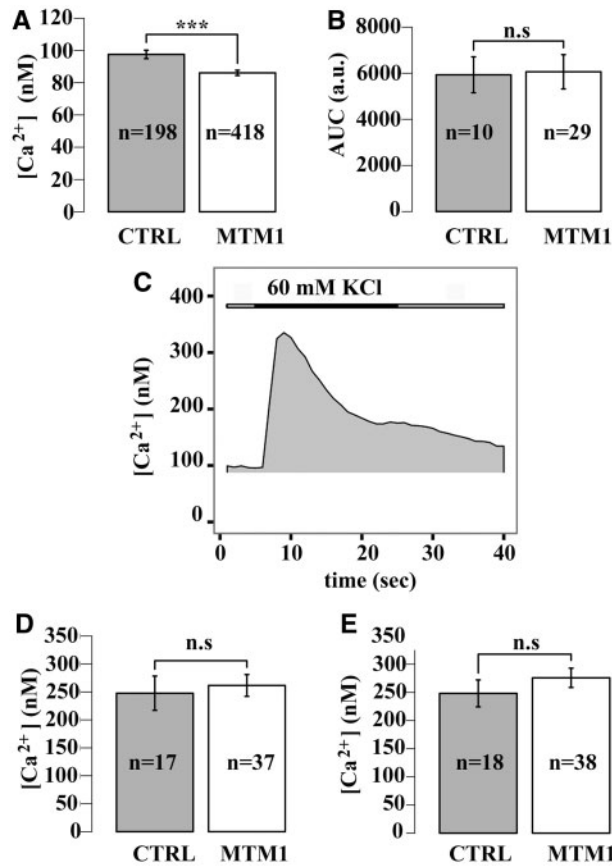
Figure 4. Calcium homeostasis in human skeletal muscle-derived myotubes from XLMTM patients and healthy controls. (**A**) Resting $[Ca^{2+}]_i$. Bars represent the mean ($\pm$SEM) resting $[Ca^{2+}]$ calculated from the indicated number of cells. Myotubes from XLMTM patients had significantly lower resting $[Ca^{2+}]_i$ than myotubes from healthy controls. ***$P < 0.001$ Student's t test. (**B**) Total amount of Ca^{2+} in the SR. Bars represent the mean ($\pm$ SEM) fluorescence obtained by calculating the Area Under the Curve (AUC) after stimulation of cells with 1 μM ionomycin + 1 μM thapsigargin in Krebs Ringer containing 0.5 mM EGTA. (**C**) Representative trace showing changes in $[Ca^{2+}]_i$ induced by stimulation with 60 mM KCl. (**D**) Peak (mean $\pm$ SEM) response to 600 μM 4-chloro-m-cresol and (**E**) 60 mM KCl. Experiments were performed as indicated in the Materials and Methods section in Krebs-Ringer containing 100 μM La^{3+} unless otherwise stated. n.s. results were not significantly different.

is visible in homogenates from the foetal muscles. A band showing immunoreactivity with anti-MyHC3 antibodies is present in the muscle biopsy from patient MTM1 6212 but not with biopsies from patients MTM1 0805,1816 and 0078 indicating that the latter patients do not express detectable levels of embryonic/foetal MyHC.

Discussion

In the present study, we investigated skeletal muscle samples from 6 patients affected by XLMTM and assessed the impact of *MTM1* mutations on ECC. Our results show that *MTM1* mutations do not directly impinge on ECC since at the level of myotubes the absence of myotubularin does not significantly affect calcium homeostasis but rather affects cell morphology and size. This contrasts with what is observed in mature muscle fibres, where the expression of key proteins involved in ECC is significantly down-regulated. In addition, we show that in muscles from XLMTM patients HDAC-4 is significantly up-regulated.

We propose that secondary modifications occurring as a consequence of *MTM1* mutations affect the expression of muscle-specific transcripts and are responsible at least in part for the muscle weakness seen in these patients.

In order to assess ECC we used muscle cells explanted from the patient's biopsies, an experimental model we have previously used to investigate calcium homeostasis in cells from patients affected by other congenital muscle diseases (28,34,41,42). Such a system offers several advantages, including (i) endogenous expression of the patient's mutation without the need to transfect or virally infect cells, (ii) ease with which cells are grown and differentiated into myotubes and (iii) amenability of cells for studies on basic calcium homeostasis. The main drawback of this model is that myotubes do not differentiate into fully developed muscle fibres and that they will also express, if present, other mutations present in the patient's genome. From a morphological point of view, the most striking difference was the appearance of the myotubes, their smaller size and number of nuclei, though the average number of nuclei corrected per cell area remained unchanged. This finding contrasts an earlier report suggesting that myotubes from XLMTM patients are indistinguishable as far as size, shape or nuclear distribution are concerned, compared to myotubes from healthy controls (43). Such a discrepancy may relate to the nature of the mutation, muscle of origin and growth conditions. All the myotubes used in the present study were from quadriceps and the mutations lead to undetectable levels of myotubularin, while in the study of Dorchies et al., muscle cells were obtained from different muscle tissues (leg, arm, quadriceps) and from patients with severe and mild phenotypes (43).

Although the exact causes of such morphological changes are difficult to uncover, they may relate to the accumulation of PIs within subcellular membrane domains, alterations of autophagy, or inappropriate activation of mTOR (44–48). As far as accumulation of specific PIs is concerned, myoblasts deficient in phosphoinositide phosphatases were reported to contain a two-fold increase in $PI3P/PI(3,5)P_2$, (14,37,38), a result confirmed in the present study where we also show that the PI3P content in mature muscle is significantly increased. Generally, PI lipids constitute less than 15% of the total cellular phospholipids with PI4P and $PI(4,5)P_2$ representing the major forms in mammalian cells (35,44,45). Thus while it is true that PI can be metabolically interconverted *in vitro*, different PI species are not equally present within the cell, do not share the same subcellular distribution and can diffuse within but not between membranes unless assisted by specific transfer proteins. For example $PI(4,5)P_2$ and $PI(3,4,5)P_3$ are concentrated in the plasma membrane, $PI(3,4)P_2$ is in the plasma membrane as well as early endocytic vesicles and PI3P is concentrated in early endosomes (35,45). Thus accumulation of PI3P as caused by *MTM1* mutations, could potentially interfere with early endosomal trafficking as recently confirmed by Ketel and co-workers (20).

An alternative possibility is that PI3P accumulation affects autophagy since this lipid plays a major role in the initiation of, and modulation of autophagy (47,48) or affects the IGF1R/AKT pathway that closely controls mTOR activation and thus cell growth, which was shown to be dysregulated in muscles from *Mtm1-/-* mice (49).

One of the main questions relating to PI metabolism and disease pathomechanism(s) is whether there is a functional link between alterations of phospholipid metabolism and skeletal muscle function. This is particularly relevant since patients carrying mutations in genes encoding enzymes involved in lipid metabolism have a muscle-specific phenotype. Recent data
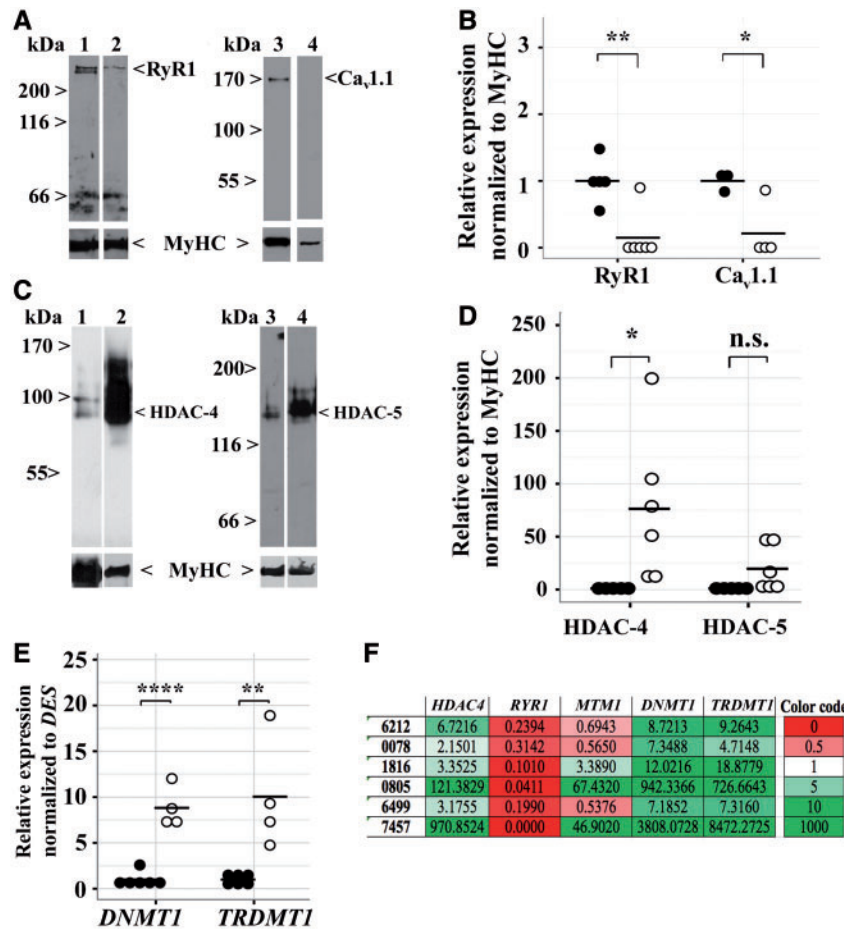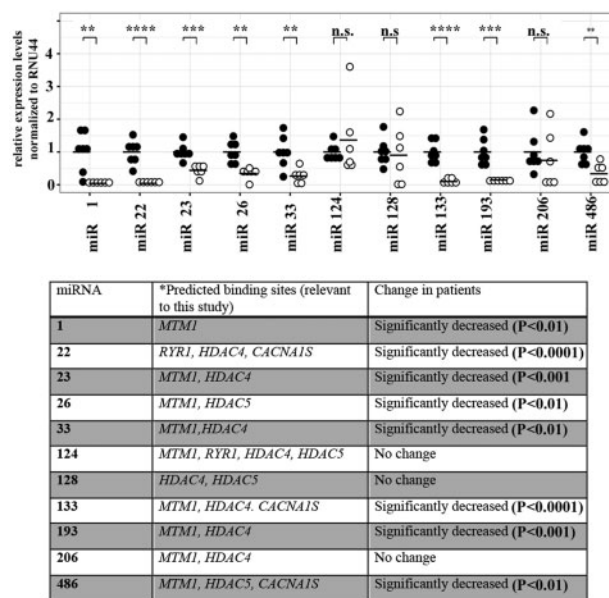
Figure 5. Western blot analysis, protein quantification and qPCR analysis of the two main calcium channels involved in skeletal muscle EC coupling, of class II HDACs and DNA methyltransferases in muscle biopsies from XLMTM patients and healthy controls. (**A**) and (**C**) Representative immunoblots probed with the indicted antibodies. Lanes 1 and 3, muscle extracts from a healthy control, lanes 2 and 4, muscle extracts from an XLMTM patient. Lower blots show immunoreactivity to an antibody recognizing all MyHC isoform used to normalize for protein loading. (**B**) and (**D**) Comparison of the relative expression of the indicated proteins in muscle extracts of the available patients; healthy controls (full circles), XLMTM patients (empty circles). Statistical analysis was performed using the Welch two sample test. $^{*}P < 0.05$ and $^{**}P < 0.01$. (**E**) Transcript levels of the DNA methylating enzymes *DNMT1* and *TRDMT1* (previously known as *DNMT2*) were significantly elevated in muscles of patients versus controls. (**F**) Gene expression was performed by qPCR as described in the Materials and Methods section and with the primer sequences given in Supplementary Material, Table S4. Each reaction was performed in triplicate on muscle biopsies from healthy controls and XLMTM patients and expression levels were normalized to *DES*. Results were prepared using Excel's 'Conditional Formatting Plugin' using the 3-scale color specified in the last column. Relative transcript content in patients was compared to that found in healthy controls that was set to 1.

support a direct effect of certain PI lipids on calcium homeostasis. In particular (i) myotubes from mice deficient in MTMR14 exhibit spontaneous Ca^{2+} leak due to the binding of $PI(3,5)P_2$ and $PI(3,4)P_2$ to RyR1 which promotes its activation (14); (ii) PI3P and $PI(3,5)P_2$, directly depress voltage activated Ca^{2+} release when injected into mouse FDB fibres (50); (iii) depletion of $PI(4,5)P_2$ in the transverse tubules impairs SR Ca^{2+} release (51) and (iv) the endoplasmic reticulum and sarcoplasmic reticulum of animal models knocked out for *MTM1* and *MTMR14* show profound structural changes and dysfunction of ECC (13,14,23,38). For these reasons, we were surprised to find that the calcium homeostasis and ECC of myotubes from patients with *MTM1* mutations were similar to those of control myotubes. Indeed, we observed no changes in the levels of the SR Ca^{2+} stores, nor in the peak Ca^{2+} elicited by depolarization or by direct pharmacological activation of the RyR1. We did observe a small decrease in the resting $[Ca^{2+}]_i$ but this is most likely due to the degree of differentiation of the myotubes rather than to a direct effect on ECC. In fact, Western blot analysis showed that myotubes from the XLMTM patients express higher levels of RyR1 and $Ca_v1.1$

compared to control myotubes, though the subcellular localization of both proteins was similar in patient and control cells. Importantly, the lack of effect on Ca^{2+} homeostasis is not due to the lack of myotubularin expression at the level of the myotubes as opposed to mature muscle, since Western blot analysis showed that the immunopositive band was present in protein extracts of myotubes from controls (but not from patients).

This observed lack of effect of *MTM1* mutations on the ECC of myotubes was puzzling especially considering that muscle biopsies from the same patients and muscles from the *Mtm1-/-* mice showed significantly lower levels of RyR1 and $Ca_v1.1$ proteins and that FDB fibres from the *Mtm1-/-* mice showed a much smaller depolarization induced peak Ca^{2+} transient compared to their wild type littermates (23). This apparent inconsistency between myotubes and mature muscle fibres indicates that: (i) the lack of myotubularin does not directly affect ECC and (ii) requires fully developed mature fibres in order to show a functional effect. This is reminiscent of what occurs in muscles from patients with recessive *RYR1* mutations, where no apparent effect on Ca^{2+} homeostasis was seen at the myotube level

miRNA	*Predicted binding sites (relevant to this study)	Change in patients
1	*MTM1*	Significantly decreased (P<0.01)
22	*RYR1, HDAC4, CACNA1S*	Significantly decreased (P<0.0001)
23	*MTM1, HDAC4*	Significantly decreased (P<0.001)
26	*MTM1, HDAC5*	Significantly decreased (P<0.01)
33	*MTM1,HDAC4*	Significantly decreased (P<0.01)
124	*MTM1, RYR1, HDAC4, HDAC5*	No change
128	*HDAC4, HDAC5*	No change
133	*MTM1, HDAC4. CACNA1S*	Significantly decreased (P<0.0001)
193	*MTM1, HDAC4*	Significantly decreased (P<0.001)
206	*MTM1, HDAC4*	No change
486	*MTM1, HDAC5, CACNA1S*	Significantly decreased (P<0.01)

Figure 6. qPCR analysis of selected microRNAs in muscle biopsies from healthy controls versus XLMTM patients. Top panel: each reaction was performed in triplicate on muscle biopsies from healthy controls (full circles) or XLMTM patients (empty circles). Expression levels were normalized to RNU44 expression. Bottom panel: predicted binding partner(s) of the quantified miRNA and statistical analysis (Student's t test) of changes in levels of expression between healthy controls and XLMTM patients.
Source: http://www.microrna.org/microrna/getGeneForm.do (Supplementary Material, Table 3 for more details on the miRs).

but where a significant decrease of ECC proteins in muscle homogenates was found (34). In the latter case epigenetic modifications were responsible at least in part, for the decrease in ECC protein expression. Interestingly, in muscle biopsies from the XLMTM patients *RYR1* transcript content was severely reduced, *HDAC4, DNMT1* and *TRDMT1* levels were significantly increased and most muscle-specific miRs were down-regulated. Although in the present study the sample number was too small to draw definite conclusions and make specific correlations, they may explain phenotypic differences observed in patients. Indeed, patients carrying mutations such as the p.R241C substitution, or patients carrying deletions of exon 1 have been reported as being severely, moderately or mildly affected (16–19) while some patients carrying nonsense mutations predicted to result in a truncated enzyme-dead protein, were surprisingly only moderately affected (18,19).

An important additional observation of the present study relates to the amounts of protein and transcript levels within the muscle biopsy that did not always match. Lack of correlation between transcripts and proteins have been reported by a number of authors and may relate to transcript/protein stability, stability of the transcript versus selected housekeeping gene, effect of post-translational modifications on protein turnover (52–55). However, lack of correlation of the same protein/transcripts in the same tissue in some individuals but not others, indicates that different mechanisms are activated in response to mutations, stress or environmental factors in different cells and that these will result in 'phenotypic variability'. One such mechanism linking the regulation of gene expression to external or environmental factors involves a group of enzymes known HDACs that can be recruited in association with DNA-methylation to repress transcription by deacetylating core

histones (56). Class II HDACs are expressed in skeletal muscle and affect myogenesis by sequestering mef2, a master transactivator of skeletal muscle gene expression (57,58). Mef2 sequestration results in blockage of mef2 dependent gene transcription, including transcription of muscle-specific miRs such as miR1 and miR133 (59,60) and this in combination with the increased expression of DNA methylating enzymes could be a contributing factor to the fast to slow fibre type conversion, triadic disarrangement and phenotype of a muscle with 'foetal-like' characteristics. Clearly, more work needs to be carried out in the future and it is important that transcriptome analysis be validated at the protein level and more detailed characterization of the MyHC isoform expressed be performed whenever possible.

Taken together the results of this and our previous study (34) raise the interesting possibility that the epigenetic modifications taking place in skeletal muscle as a consequence of mutations in different genes involved in congenital myopathies are activated and cause a general down-regulation of most skeletal muscle ECC genes and the reversal to a more 'foetal-like' muscle. It is difficult to understand how and why such epigenetic modifications are activated but they may relate to the fact that of phosphoinositide lipids have a negative effect on ECC, on SR structure and consequently on muscle function. The lack of normal Ca^{2+} homeostasis in skeletal muscle could affect its physiological development further precluding its proper function. If this is the case, then it is possible that patients with such congenital myopathies may show benefit from pharmacological compounds targeted to decrease the expression levels of class II HDACs.

Materials and Methods

Muscle biopsies and cell cultures

Human myoblasts from controls and patients were cultured in skeletal muscle growth medium as previously described (34,36,39,41) until approximately 90% confluent then they were induced to differentiate by switching the medium to differentiation medium (PromoCell; C-23061) for 7 days.

Calcium measurements

Muscle cells were cultured on laminin-coated 0.17 mm glass cover slips as previously described (34,39,42). Fully differentiated myotubes were loaded with 5 μM fura-2/AM (Calbiochem; 344905) for 30 min at 37° C and mounted on a temperature-controlled stage (tempcontrol 37-2 digital). The chamber was continuously perfused with Krebs-Ringer medium containing 2 mM Ca^{2+} and cells were stimulated using a 12-way 100 mm diameter quartz micro-manifold computer-controlled microperfuser (ALA Scientific Instruments), as described previously (39,41,42). The recordings were done on a fluorescent Axiovert S100 TV inverted microscope (Carl Zeiss) equipped with a 20x water-immersion FLUAR objective (NA 0.17) and filters (BP 340/ 380, FT 425, BP 500/530) attached to a Photometrics Cascade 128+ CCD (charge-coupled device) camera controlled by VisiView software version 2.0.8. Data analysis was performed using ImageJ version 1.50 g and the Ratio Plus, Process Fura2, Time Series Analyzer V 3 plugins.

Brightfield and confocal microscopy

Muscle cells were cultured on laminin-coated Ibid® 0.17 mm μ-Slide 4 well glass bottom slides (Ibid Cat # 80427) until 90%
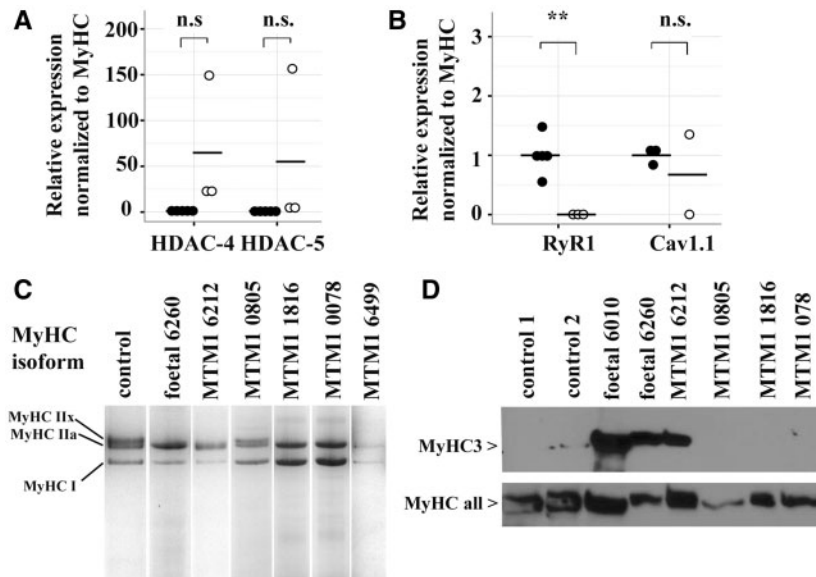
Figure 7. Muscle biopsies from foetuses express lower levels of RyR1, different MyHC isoforms and variable levels of class II HDACs compared to muscles of older healthy controls. (**A**) Quantification of HDAC-4 and HDAC-5 and (**B**) quantification of RyR1 and Ca$_v$1.1 in total muscle homogenates from healthy controls (full circles) and foetal muscles (empty circles). Statistical analysis was performed using the Welch two sample test. $**P < 0.01$; n.s. not significantly different. (**C**) Electrophoretic separation of MyHC isoforms performed according to Talmadge and Roy (40). (**D**) Representative Western blots showing the immunoreactivity of the muscle homogenates with an antibody recognizing the embryonic/foetal isoform (MyHC 3, top) and an antibody recognizing all MyHC isoforms (bottom).

confluent. The medium was switched to differentiation medium for 7 days after which cells were fixed in 4% paraformaldehyde in phosphate buffered saline (PBS) and visualized using a Nikon TE2000 TIRF microscope equipped with a 20x Plan Apo air objective and attached to an electron multiplier Hamamatsu CCD camera C9100-13.

For cell size and nuclear counting, cells were stained with 4',6-diamidino-2-phenylindole (DAPI) and observed with a Nikon A1plus confocal microscope equipped with a Plan Fluor 20x air objective (NA 0.75); calculation of the cell area was performed using the Fiji software (version 2.0.0-rc-49/1.51d) as described (61). For immunofluorescence, cells were permeabilized with 1% Triton® X-100 in PBS for non-lipophilic targets (myotubularin, RyR1, Ca$_v$1.1) and 0.01% Digitonin (Calbiochem; 300411) in TRIS buffered saline (TBS) for lipophilic targets (PI3P, PI(3,4)P$_2$). Non-specific binding sites were blocked by 1% blocking buffer in TBS (Roche; 11500694001). Cells were incubated with the primary antibodies detailed in Supplementary Material, Table S3 for 60 min at room temperature, rinsed three times with 0.1% Tween® 20 in TRIS buffered saline (TBS-T) for non-lipophilic targets; for lipophilic targets antibodies were incubated at 37 °C and washed with 0.1% blocking buffer in PBS. Cells were then incubated for 60 min at room temperature with the appropriate Alexa Fluor conjugated secondary antibodies (Life Technologies). Actin filaments were stained for 30 min using phalloidin conjugated Alexa Fluor® 647 and nuclei were counterstained with DAPI. Myotubes were visualized on a Nikon® A1plus confocal microscope equipped with a Nikon Plan Apo TIRF 60x oil objective (NA 1.49) and with Coherent® Sapphire lasers (405, 488, 561 nm) and an MPBC® CW Visible Fiber laser (647 nm) controlled by Nikon® NIS-Elements Confocal software.

Electrophoresis and immunoblotting

Total homogenates of muscle biopsies and myotubes were prepared as previously described (34,39). Protein concentration was determined using the Bradford protein assay kit (Bio-Rad,

500-0006) using bovine serum albumin as a standard. Proteins (50 µg/lane) were separated on 6 or 7.5% SDS-PAGE and blotted onto nitrocellulose. For MyHC isoform separation, gels were prepared according to Talmadge and Roy (40) and stained with Coomassie Blue R250 (Fluka; 27816). Single fibres isolated from mouse FDB or soleus fibres were used to identify the different MyHC isoforms; alternatively in order to verify whether embryonic/neonatal isoforms were present, proteins were transferred onto nitrocellulose and stained with anti-MyHC3 followed by anti-MyHC recognizing all isoforms. For immunoblotting, membranes were blocked for 60 min at room temperature or overnight at 4 °C in 1% blocking buffer (Roche; 11500694001) and incubated with the primary antibodies listed in Supplementary Material, Table S3. Secondary antibodies/proteins used were either anti-mouse peroxidase (Sigma, catalogue #A2304) or protein-G peroxidase (Sigma, catalogue # P8170). Bands were visualized using the SuperSignal Dura West kit (Thermo Scientific; 34076) or BM Chemiluminescence kit (Roche; 11520709001). For quantification, films were scanned on an Epson Perfection V700 Photo as 16-bit tiff image and densiometrically analysed using the GelAnalyzer software version 2010a.

Quantitative PCR

RNA was extracted from muscle biopsies using TRIzol® reagent (Thermo Fischer; 15596026) according to the manufacturer's instructions. DNA was removed using DNase I (Invitrogen; 18068-015) and 1000 ng RNA were reverse-transcribed into cDNA using the High capacity cDNA Reverse Transcription Kit (Applied Biosystems; 4368814) on an Applied Biosystems 2720 Thermal Cycler. The cDNA was amplified by quantitative real-time polymerase chain reaction (qPCR) using either Power Sybr® Green Master Mix (Applied Biosystems; 4367659) for regular DNA quantification or TaqMan® microRNA reverse transcription kit (Applied Biosystems; 4366596) for miRNA assays both on an Applied Biosystems 7500 Fast Real-time PCR System running 7500 software version 2.3 (34). Quantification was based on the

comparative ΔΔCt method. The sequences of the primers used for qPCR are listed in Supplementary Material, Table S4 and the sequences of primers used for miRNA quantification are listed in Supplementary Material, Table S5. Each reaction was performed in triplicate and results are expressed as relative gene expression normalized to desmin (*DES*) for qPCR and to the human housekeeping gene RNU44 for miRNAs. Expression levels obtained from biopsies of healthy controls were set to 1.

PIP lipid quantification

The content of PI3P and PI(4,5)P$_2$ was determined on muscle biopsies from patients and controls using the Mass ELISA kits (Echelon catalogue numbers K-3300 and K-4500), following the manufacturer's recommendations. For each muscle, the content of PI3P was calculated either as [PI3P] per gram of wet weight or was normalized to the content of PI(4,5)P$_2$ which is reported to be constant in most tissues (62).

Compliance with ethical standards

All procedures performed in studies involving human participants were in accordance with the ethical standards of the institutional and/or national research committee and with the 1964 Helsinki declaration and its later amendments or comparable ethical standards. This study was approved by the Ethikkommission beider Basel (permit N° EK64/12); all subjects gave written informed consent to carry out this work.

Statistical analysis

Statistical analysis was performed using the 'R' version 3.2.4 running on platform x86_64-apple-darwin13.4.0 (64-bit). For dose-response curves the package 'drc' version 2.5–12 was used (63). Comparisons of two groups were performed using the Student's *t*-test, for groups of three or more comparisons were made using the ANOVA test followed by the Bonferroni post-hoc test unless otherwise stated. Means were considered statistically significant when P values were < 0.05. All figures were created using Adobe Photoshop CS6 or R Studio (version 0.99.891 or newer).

Supplementary Material

Supplementary Material is available at *HMG* online.

References

1. Wallggren-Pettersson, C., Clarke, A., Samson, F., Fardeau, M., Dubowitz, V., Moser, H., Grimm, T., Barohn, R.J. and Barth, P.G. (1995) The myotubular myopathies: differential diagnosis of the X-linked recessive, autosomal dominant, and autosomal recessive forms and present state of DNA studies. *J. Med. Genet.*, **32**, 673–679.

2. Laporte, J., Hu, L.J., Kretz, C., Mandel, J.L., Kioschis, P., Coy, J.F., Klauck, S.M., Poustka, A. and Dahl, N. (1996) A gene mutated in X-linked myotubular myopathy defines a new putative tyrosine phosphatase family conserved in yeast. *Nat. Genet.*, **13**, 175–182.

3. Hnia, K., Vaccari, I., Bolino, A. and Laporte, J. (2012) Myotubularin phosphoinositide phosphatases: cellular functions and disease pathophysiology. *Trends. Mol. Med.*, **18**, 317–327.

4. Durieux, A.C., Vignaud, A., Prudhon, B., Viou, M.T., Beuvin, M., Vassilopoulos, S., Fraysse, B., Ferry, A., Lainé, J., Romero, N.B., *et al.* (2010) A centronuclear myopathy-dynamin 2 mutation impairs skeletal muscle structure and function in mice. *Hum. Mol. Genet.*, **15**, 4820–4836.

5. Adam, J., Basnet, N. and Mizuno, N. (2015) Structural insights into the cooperative remodeling of membranes by amphiphysin/BIN1. *Sci. Rep.* 10.1038/srep15452,

6. Böhm, J., Biancalana, V., Malfatti, E., Dondaine, N., Koch, C., Vasli, N., Kress, W., Strittmatter, M., Taratuto, A.L., Gonorazky, H., *et al.* (2014) Adult-onset autosomal dominant centronuclear myopathy due to BIN1 mutations. *Brain*, **137**, 3160–3170.

7. Ceyhan-Birsoy, O., Agrawal, P.B., Hidalgo, C., Schmitz-Abe, K., DeChene, E.T., Swanson, L.C., Soemedi, R., Vasli, N., Iannaccone, S.T., Shieh, P.B., *et al.* (2013) Recessive truncating titin gene, TTN, mutations presenting as centronuclear myopathy. *Neurology*, **81**, 1205–1214.

8. Barth, P.G. and Dubowitz, V. (1998) X-linked myotubular myopathy: a long term follow-up study. *Eur. J. Paediatr. Neurol.*, **1**, 49–56.

9. Buj-Bello, A., Biancalana, V., Moutou, C., Laporte, J. and Mandel, J.L. (1999) Identification of novel mutations in the MTM1 gene causing severe and mild forms of X-linked myotubular myopathy. *Hum. Mutat.*, **14**, 320–325.

10. Abath Neto, O., Silva, M.R., Martins Cde, A., Oliveira Ade, S., Reed, U.C., Biancalana, V., Pesquero, J.B., Laporte, J. and Zanoteli, E. (2016) A study of a cohort of X-linked myotubular myopathy at the clinical, histologic, and genetic levels. *Pediatr. Neurol.*, **58**, 107–112.

11. Romero, N.B. and Bitoun, M. (2011) Centronuclear myopathies. *Semin. Pediatr. Neurol.*, **18**, 250–256.

12. Sewry, C.A., Jimenez-Mallebrera, C. and Muntoni, F. (2008) Congenital myopathies. *Curr. Opin. Neurol.*, **21**, 569–575.

13. Dowling, J.J., Vreede, A.P., Low, S.E., Gibbs, E.M., Kuwada, J.Y., Bonnemann, C.G. and Feldman, E.L. (2009) Loss of myotubularin function results in T-tubule disorganization in zebrafish and human myotubular myopathy. *PLoS. Genet.*, 10.1371/journal.pgen.1000372.

14. Shen, J., Yu, W.M., Brotto, M., Scherman, J.A., Guo, C., Stoddard, C., Nosek, T.M., Valdivia, H.H. and Qu, C.K. (2009) Deficiency of MIP/MTMR14 phosphatase induces a muscle disorder by disrupting Ca^{2+} homeostasis. *Nat. Cell Biol.*, **11**, 769–776.

15. Sarnat, H.B. (1990) Myotubular myopathy: arrest of morphogenesis of myofibres associated with persistence of fetal vimentin and desmin. Four cases compared with fetal and neonatal muscle. *Can. J. Neurol. Sci.*, **17**, 109–123.

16. Biancalana, V., Caron, O., Gallati, S., Baas, F., Kress, W., Novelli, G., D'Apice, M.R., Lagier-Tourenne, C., Buj-Bello, A., Romero, N.B. and Mandel, J.L. (2003) Characterisation of mutations in 77 patients with X-linked myotubular myopathy, including a family with a very mild phenotype. *Hum. Genet.*, **112**, 135–142.

17. Herman, G., Kpüacz, K., Zhao, W., Mills, P.L., Metzenberg, A. and Das, S. (2002) Characterization of Mutations in Fifty North American Patients With X-linked Myotubular Myopathy. *Hum. Mutat.*, **19**, 114–121.

18. McEntagart, M., Parsons, G., Buj-Bello, A., Biancalana, V., Fenton, I., Little, M., Krawczak, M., Thomas, N., Herman, G., Clarke, A. and Wallgren-Pettersson, C. (2003) Genotype-phenotype correlations in X-linked myotubular myopathy. *Neuromuscul. Disord.*, **12**, 939–946.

19. Laporte, J., Biancalana, V., Tanner, S.M., Kress, W., Schneider, V., Wallgren-Pettersson, C., Herger, F., Buj-Bello, A., Blondeau, F., Liechti-Gallati, S. and Mandel, J.L. (2000) MTM1 mutations in X-linked myotubular myopathy. *Hum. Mutat.*, **15**, 393–409.

20. Ketel, K., Krauss, M., Nicot, A.S., Puchkov, D., Wieffer, M., Müller, R., Subramanian, D., Schultz, C., Laporte, J. and Haucke, V. (2016) A phosphoinositide conversion mechanism for exit from the endosome. *Nature*, **529**, 408–412.

21. Hnia, K., Tronchère, H., Tomczak, K.K., Amoasii, L., Schultz, P., Beggs, A.H., Payrastre, B., Mandel, J.L. and Laporte, J. (2011) Myotubularin controls desmin intermediate filament architecture and mitochondrial dynamics in human and mouse skeletal muscle. *J. Clin. Invest.*, **121**, 70–85.

22. Robinson, F.L. and Dixon, J.E. (2006) Myotubularin phosphatases: policing 3-phosphoinostides. *Trends Cell Biol.*, **16**, 403–412.

23. Al-Qusairi, L., Weiss, N., Toussaint, A., Berbey, C., Massaddeq, N., Kretz, C., Sanoudou, D., Beggs, A.H., Allard, B., Mandel, J.L., *et al.* (2009) T-tubule disorganization and defective excitation-contraction coupling in muscle fibers lacking myotubularin lipid phosphatase. *Proc. Natl. Acad. Sci. U.S.A*, **106**, 18763–18768.

24. Franzini-Armstrong, C. and Protasi, F.G. (1997) Ryanodine receptors of striated muscles: a complex channel capable of multiple interactions. *Physiol. Rev.*, **77**, 699–729.

25. Rios, E. and Pizarro, G. (1991) Voltage sensor of excitation contraction coupling in skeletal muscle. *Physiol. Rev.*, **71**, 849–908.

26. Catterall, W.A. (2011) Voltage gated calcium channels. *Cold Spring Harb. Perspect. Biol.*, 10.1101/cshperspect.a003947.

27. Franzini-Armstrong, C. and Jorgensen, A.O. (1994) Structure and development of E-C coupling units in skeletal muscle. *Annu. Rev. Physiol.*, **56**, 509–534.

28. Zhou, H., Jungbluth, H., Sewry, C.A., Feng, L., Bertini, E., Bushby, K., Straub, V., Roper, H., Rose, M.R., Brockington, M., *et al.* (2007) Molecular mechanisms and phenotypic variation in RYR1-related congenital myopathies. *Brain*, **130**, 2024–2036.

29. Wilmhurst, J.M., Lillis, S., Zhou, H., Pillay, K., Henderson, H., Kress, W., Müller, C.R., Ndondo, A., Cloke, V., Cullup, T., *et al.* (2010) RYR1 mutations are a common cause of congenital myopathies with central nuclei. *Ann. Neurol.*, **68**, 717–726.

30. Clarke, N.E., Waddell, L.B., Cooper, S.T., Perry, M., Smith, R.L., Kornberg, A.J., Muntoni, F., Lillis, S., Straub, V., Bushby, K., *et al.* (2012) Recessive mutations in RYR1 are a common cause of congenital fiber type disproportion. *Hum. Mutat.*, **31**, E1544–E1550.

31. Komazaki, S., Ito, K., Takeshima, H. and Nakamura, H. (2002) Deficiency of triad formation in developing skeletal muscle cells lacking junctophilin type 1. *FEBS. Lett.*, **524**, 225–229.

32. Van, B., Nishi, M., Komazaki, S., Ichimura, A., Kakizawa, S., Nakanaga, K., Aoki, J., Park, K.H., Ma, J., Ueyama, T., *et al.* (2007) Mitsugumin 56 is a sarcoplasmic reticulum-resident protein essential for postnatal muscle maturation. *FEBS Lett.*, **589**, 1095–1104.

33. Delbono, O., Xia, J., Treves, S., Wang, Z.M., Jimenez-Moreno, R., Payne, A.M., Messi, M.L., Briguet, A., Schaerer, F., Nishi, M., *et al.* (2007) Loss of skeletal muscle strength by ablation of the sarcoplasmic reticulum protein JP45. *Proc. Natl. Acad. Sci. U.S.A*, **104**, 20108–20113.

34. Rokach, O., Sekulic-Jablanovic, M., Voermans, N., Wilmshurst, J., Pillay, K., Heytens, L., Zhou, H., Muntoni, F., Gautel, M., Nevo, Y., *et al.* (2015) Epigenetic changes as a common trigger of muscle weakness in congenital myopathies. *Hum. Mol. Genet.*, **24**, 4636–4647.

35. Di Paolo, G. and DeCamilli, P. (2006) Phosphoinositides in cell regulation and membrane dynamics. *Nature*, **443**, 651–657.

36. Rokach, O., Ullrich, N.D., Rausch, M., Mouly, V., Zhou, H., Muntoni, F., Zorzato, F. and Treves, S. (2013) Establishment of a human skeletal muscle-derived cell line: biochemical, cellular and electrophysiological characterization. *Biochem. J.*, **455**, 169–177.

37. Pierson, C.R., Dulin-Smith, A.N., Durban, A.N., Marshall, M.L., Marshall, J.T., Snyder, A.D., Naiyer, N., Gladman, J.T., Chandler, D.S., Lawlor, M.W., *et al.* (2012) Modeling the human MTM1 p.R69C mutation in murine Mtm1 results in exon 4 skipping and a less severe myotubular myopathy phenotype. *Hum. Mol. Genet.*, **21**, 811–825.

38. Amoasii, L., Hnia, K., Chicanne, G., Brech, A., Cowling, B.S., Müller, M.M., Schwab, Y., Koebel, P., Ferry, A., Payrastre, B. and Laporte, J. (2013) Myotubularin and PtdIns3P remodel the sarcoplasmic reticulum in muscle in vivo. *J. Cell Sci.*, **126**, 1806–1819.

39. Sekulic-Jablanovic, M., Palmowski-Wolfe, A., Zorzato, F. and Treves, S. (2015) Characterization of excitation-contraction coupling components in human extraocular muscles. *Biochem. J.*, **466**, 29–36.

40. Talmadge, R.J. and Roy, R.R. (1985) Electrophoretic separation of rat skeletal muscle myosin heavy chain isoforms. *J. Appl. Physiol.*, **75**, 2337–2340.

41. Zhou, H., Yamaguchi, N., Xu, L., Wang, Y., Sewry, C., Jungbluth, H., Zorzato, F., Bertini, E., Muntoni, F., Meissner, G. and Treves, S. (2006) Characterization of recessive RYR1 mutations in core myopathies. *Hum. Mol. Genet.*, **16**, 2791–2803.

42. Ducreux, S., Zorzato, F., Müller, C., Sewry, C., Muntoni, F., Quinlivan, R., Restagno, G., Girard, T. and Treves, S. (2004)

Effect of ryanodine receptor mutations on interleukin-6 release and intracellular calcium homeostasis in human myotubes from malignant hyperthermia-susceptible individuals and patients affected by central core disease. *J Biol. Chem.*, **279**, 43838–43846.

43. Dorchies, O.M., Laporte, J., Wagner, S., Hindelang, C., Warter, J.M., Mandel, J.L. and Poindron, P. (2011) Normal innervation and differentiation of X-linked myotubular myopathy muscle cells in a nerve-muscle coculture system. *Neuromuscul. Disord.*, **11**, 736–746.

44. Balla, T. (2013) Phosphoinosities: tiny lipids with giant impact on cell regulation. *Physiol. Rev.*, **93**, 1019–1137.

45. Billcliff, P.G. and Mowe, M. (2014) Inositol lipid phosphatases in membrane trafficking and human diseases. *Biochem. J.*, **461**, 159–175.

46. Vergne, I., Elmaoued, R.A., Tosch, V., Delgado, M.A., Proikas-Cezanne, T., Laporte, J. and Deretic, V. (2009) Control of autophagy initiation by phosphoinositide 3-phosphatese Jumpy. *embo. J.*, **28**, 2244–2258.

47. Vergne, I. and Deretic, V. (2010) The role of PI3Phosphatases in the regulation of autophagy. *FEBS. Lett.*, **584**, 1313–1318.

48. Jung, C.H., Ro, S.H., Cao, J., Otto, N.M. and Kim, D.H. (2010) mTOR regulation of autophagy. *FEBS. Lett.*, **584**, 1287–1295.

49. Al-Qusairi, L., Prokic, I., Amoasii, L., Kretz, C., Messaddeq, N., Mandel, J.L. and Laporte, J. (2013) Lack of myotubularin (MTM1) leads to muscle hypotrophy through unbalanced regulation of the autophagy and ubiquitin-proteasome pathways. *Faseb. J.*, **27**, 3384–3394.

50. Rodríguez, E.G., Lefebvre, R., Bodnár, D., Legrand, C., Szentesi, P., Vincze, J., Poulard, K., Bertrand-Michel, J., Csernoch, L., Buj-Bello, A. and Jacquemond, V. (2014) Phosphoinositide substrates of myotubularin affect voltage-activated Ca^{2+} release in skeletal muscle. *Pflügers. Arch.*, **465**, 973–985.

51. Berthier, C., Kutchukian, C., Bouvard, C., Okamura, Y. and Jacquemond, V. (2015) Depression of voltage-activated Ca^{2+} release in skeletal muscle by activation of a voltage-sensing phosphatase. *J. Gen. Physiol.*, **145**, 315–330.

52. Hause, R.J., Stark, A.L., Antao, N.N., Gorsic, L.K., Chung, S.H., Brown, C.D., Wong, S.S., Gill, D.F., Myers, J.L., To, L.A., *et al.* (2014) Identification and validation of genetic variants that influence transcription factor and cell signaling protein levels. *Am. J. Hum. Genet.*, **95**, 194–208.

53. Tian, Q., Stepaniants, S.B., Mao, M., Weng, L., Feetham, M.C., Doyle, M.J., Yi, E.C., Dai, H., Thorsson, V., Eng, J., *et al.* (2004) Integrated genomic and proteomic analyses of gene expression in Mammalian cells. *Mol. Cell. Proteomics*, **3**, 960–969.

54. Vogel, C., Abreu Rde, S., Ko, D., Le, S.Y., Shapiro, B.A., Burns, S.C., Sandhu, D., Boutz, D.R., Marcotte, E.M. and Penalva, L.O. (2010) Sequence signatures and mRNA concentration can explain two-thirds of protein abundance variation in a human cell line. *Mol. Syst. Biol*, **6**, 400. 10.1038/msb2010.59.

55. Vogel, C. and Marcotte, E.M. (2012) Insights into the regulation of protein abundance from proteomic and transcriptomic analyses. *Nat. Rev. Genet.*, **13**, 227–132.

56. Workmann, J.L. and Kingston, R.E. (1998) Alteration of nucleosome structure as a mechanism of transcriptional regulation. *Annu. Rev. Biochem.*, **67**, 545–579.

57. Lu, J., McKinsey, T.A., Zhang, C.L. and Olson, E.N. (2000) Regulation of skeletal myogenesis by association of the mef2 transcription factor with class II Histone deacetylases. *Mol. Cell*, **6**, 233–244.

58. Naya, F.J. and Olson, E.N. (1999) MEF2: a transcriptional target for signaling pathways controlling skeletal muscle growth and differentiation. *Curr. Opin. Cell Biol.*, **11**, 683–688.

59. McKinsey, T.A., Zhang, C.L., Lu, J. and Olson, E.N. (2000) Signal-dependent nuclear export of a histone deacetylase regulates muscle differentiation. *Nature*, **408**, 106–111.

60. Liu, N., Williams, A.H., Kim, Y., McAnally, J., Bezprozvannaya, S., Sutherland, L.B., Richardson, J.A., Bassel-Duby, R. and Olson, E.N. (2007) An intragenic MEF2-dependent enhancer directs muscle-specific expression of microRNAs 1 and 133 Mef2 and myomesin. *Proc. Natl. Acad. Sci. U.S.A*, **104**, 20844–20849.

61. McCloy, R.A., Rogers, S., Caldon, C.E., Lorca, T., Castro, A. and Burgess, A. (2014) Partial inhibition of Cdk1 in G2 phase overrides the SAC and decouples mitotic events. *Cell Cycle*, **13**, 1400–1412.

62. Costa, C., Ebi, H., Martini, M., Beausoleil, S.A., Faber, A.C., Jakubik, C.T., Huang, A., Wang, Y., Nishtala, M., Hall, B., *et al.* (2015) Measurement of PIP3 levels reveals an unexpected role for p110beta in early adaptive responses to p110alpha-specific inhibitors in luminal breast cancer. *Cancer Cell*, **27**, 97–108.

63. Ritz, C., Baty, F., Streibig, J.C. and Gerhard, D. (2015) Dose-Response Analysis Using R. *PLoS One*, doi: 10.1371/journal.pone.0146021.